Acta Neuropathol (2014) 127:257–270
DOI 10.1007/s00401-013-1215-5

ORIGINAL PAPER

Soluble pathological tau in the entorhinal cortex leads to presynaptic deficits in an early Alzheimer's disease model

Manuela Polydoro · Volodymyr I. Dzhala · Amy M. Pooler · Samantha B. Nicholls · A. Patrick McKinney · Laura Sanchez · Rose Pitstick · George A. Carlson · Kevin J. Staley · Tara L. Spires-Jones · Bradley T. Hyman

Received: 23 April 2013 / Revised: 28 October 2013 / Accepted: 9 November 2013 / Published online: 24 November 2013

Abstract Neurofibrillary tangles (NFTs), a hallmark of Alzheimer's disease, are intracellular silver and thioflavin S-staining aggregates that emerge from earlier accumulation of phospho-tau in the soma. Whether soluble misfolded but nonfibrillar tau disrupts neuronal function is unclear. Here we investigate if soluble pathological tau, specifically directed to the entorhinal cortex (EC), can cause behavioral or synaptic deficits. We studied rTgTauEC transgenic mice, in which P301L mutant human tau overexpressed primarily in the EC leads to the development of tau pathology, but only rare NFT at 16 months of age. We show that the early tau lesions are associated with nearly normal performance in contextual fear conditioning, a hippocampal-related behavior task, but more robust changes in neuronal system activation as marked by *Arc* induction and clear electrophysiological defects in perforant pathway synaptic plasticity. Electrophysiological changes were likely due to a presynaptic deficit and changes in probability of neurotransmitter release. The data presented here support the hypothesis that misfolded and hyperphosphorylated tau can impair neuronal function within the entorhinal-hippocampal network, even prior to frank NFT formation and overt neurodegeneration.

Keywords Tau · *Arc* induction · Synaptic dysfunction · Alzheimer's disease

Introduction

Neurofibrillary tangles (NFTs), intracellular aggregates of misfolded and hyperphosphorylated tau protein, are a neuropathological feature of Alzheimer's disease (AD) and other tauopathies. In AD, NFTs correlate well with amounts of phospho-tau immunoreactivity, synapse loss, and neuronal loss. Each of these markers correlates well with dementia severity [21] so that the contribution of NFTs or phospho-tau, as opposed to neuronal or synaptic loss, cannot be discerned. Distinguishing the roles of soluble and fibrillar tau is equally difficult. Indeed, recent studies suggest that more soluble forms of tau, rather than fibrillar tangles, may be involved in neuronal dysfunction [28, 29, 44, 45, 50, 63]. We now take advantage of a recently developed mouse model with focal tau expression largely limited to the entorhinal cortex (EC) to examine the consequences of the accumulation of soluble tau and evaluate its effects on neural system integrity at a time point prior to anatomical neurodegenerative changes.

The layer II entorhinal cortex (EC-II) neurons that project to the hippocampus, via the perforant pathway (PP), are critical for memory function. They also are the first cortical

Electronic supplementary material The online version of this article (doi:10.1007/s00401-013-1215-5) contains supplementary material, which is available to authorized users.

M. Polydoro · V. I. Dzhala · A. M. Pooler · S. B. Nicholls · L. Sanchez · K. J. Staley · T. L. Spires-Jones · B. T. Hyman (✉)
Department of Neurology, Massachusetts General Hospital, Harvard Medical School, 114 16th Street Room 2009, Charlestown, MA 02129, USA
e-mail: bhyman@partners.org

A. M. Pooler
Department of Neuroscience, Institute of Psychiatry, King's College London, DeCrespigny Park, London SE5 8AF, UK

A. P. McKinney
NeuroBehavior Laboratory Core, Harvard NeuroDiscovery Center, Boston, MA 02115, USA

R. Pitstick · G. A. Carlson
McLaughlin Research Institute, Great Falls, MT 59405, USA

neurons to be affected by NFTs in AD [4, 20]. In the present study we examine the recently characterized rTgTauEC transgenic mouse in which P301L human mutant tau is overexpressed primarily in the EC, leading to pathological tau inclusions in the EC-II as animals age [9]. These animals thus mimic, from an anatomical perspective, the types of lesions that occur in very early AD and provide a platform to test the hypothesis that development of pathological tau in the EC, at a pre-tangle stage, results in memory deficits or synaptic dysfunction. We found that restricted accumulation of pathological tau in the EC and perforant pathway, prior to tangles, synaptic loss, or neuronal loss, allows nearly normal performance on hippocampal-related behavior tasks, but more marked changes in hippocampal neural system activation as indicated by *Arc* induction and defects in hippocampal electrophysiological properties. These observations implicate disturbance of synaptic transmission and plasticity in the perforant pathway at an age prior to the development of fibrillar tau aggregates (i.e. NFTs), synaptic or neuronal loss, providing evidence that favors the idea that soluble, misfolded tau can impact neural system function.

Materials and methods

Animals

rTgTauEC mice: We generated transgenic animals (called rTgTauEC—for reversible tau restricted to entorhinal cortex) by crossing FVB-Tg(tetO-TauP301L) 4510 mice [47] with a transgenic mouse line on a C57BL/6 genetic background expressing tetracycline transactivator under the control of the Klk8 neuropsin promoter (EC-tTa) that was developed at the Scripps Research Institute [62]. F1 offspring were used as experimental animals ensuring a uniform 50:50 mix of FVB and C57BL/6 genetic background. Inheritance of both the responder and activator transgenes (designated rTgTauEC) results in P301L mutant tau expression constrained to layer II of the EC and pre and para subiculum. Notably, the restricted expression of the transgene has been characterized by three independent groups [9, 18, 35]. The limited anatomical expression of the transgene was unquestionably confirmed using definitive laser capture microdissection and RT-PCR that the tau mRNA is not detectable in the DG of rTgTauEC mice [9].

Age-matched littermates expressing only the activator transgene were used as human tau-negative controls. rTgTauEC and control mice were identified by PCR screening using the primer pairs 5′-ACCTGGACATGCTGT GATAA-3′ and 5′-TGCTCCCATTCATCAGTTCC-3′ for activator transgenes [62], and 5′-TGAACCAGGATGGCT GAG CC-3′ and 5′-TTGTCATCGCTTCCAGTCCCCG-3′ for responder transgenes [9, 47]. All animal experiments were performed in accordance with national guidelines (National Institutes of Health) and approved by Massachusetts General Hospital and McLaughlin Institute Institutional Animal Care and Use Committees.

Immunohistochemistry

Standard immunofluorescence techniques were used. Briefly, animals were killed by CO_2 inhalation and brains flash-frozen in M-1 mounting medium (Shandon, Thermo Scientific); horizontal cryostat sections were cut at 10 μm, fixed in 4 % paraformaldehyde for 10 min, and permeabilized by 20 min incubation in 0.1 % Triton solution. After blocking in 5 % normal goat serum (NGS) for 1 h, the appropriate primary antibody was applied in 5 % NGS, and sections were incubated overnight at 4 °C. The antibody Tau13 which recognizes the amino acid residues 20–35 on the longest isoform of human tau [2, 25] (Covance; 1:1,000) was used to detect human tau; the conformation-specific Alz50 and MC1 antibodies (courtesy Peter Davies, Albert Einstein College of Medicine; 1:50) [3, 5, 30] used to detect misfolded tau, and PHF1 (pSer396/404) [17, 39] (courtesy Peter Davies, Albert Einstein College of Medicine; 1:500) and MC1 [23, 57] (courtesy Peter Davies, Albert Einstein College of Medicine; 1:200) or Gallyas silver staining was used to detect neurofibrillary tangles. Sections were washed and incubated with Fluorescent Alexa Fluor 488 (Jackson ImmunoResearch; 1:250) secondary antibody in 5 % NGS for 1 h at room temperature and stained with DAPI. (1:1,000).

Gallyas silver staining

Gallyas silver staining was performed as described previously [15]. Images for figures were collected on an upright Olympus BX51 microscope (Olympus America, Center Valley, PA, USA) with a 40× objective.

Densities of human tau, Alz50 and Gallyas-stained cells

The layer II of the EC and the DG were outlined on five sections per mouse ($n = 3$ per group) using Image J. Tau13, Alz50 and Gallyas-positive neurons were counted and the density of EC or DG neurons positive for each marker was calculated by dividing the number of total counted neurons by the size of the area outlined (EC or DG) in each section. The five sections from each animal were averaged for the mean value per animal. Finally, the mean value of all animals was calculated and values are presented as mean ± SEM.

Western blot analysis

Western blot analysis was performed as described previously [9]. Brains were homogenized in RIPA buffer

(Invitrogen) supplemented with a cocktail of protease and phosphatase inhibitors (Roche). Samples were homogenized using a Polytron and the protein content was determined by BCA protein assay (Thermo Scientific). The materials for SDS-PAGE were obtained from Invitrogen (NuPAGE system). Protein lysates were boiled in sample buffer consisting of lithium dodecyl sulfate sample buffer and reducing agent and resolved on 4–12 % Bis–Tris polyacrylamide precast gels in MES SDS running buffer. 30 μg of protein was loaded per lane, proteins were transferred onto nitrocellulose membrane Protran (Whatman) in transfer buffer containing 20 % methanol. Blots were blocked in Odyssey blocking buffer (Li-Cor biosciences), followed by incubation with primary antibodies (β-actin [mouse monoclonal antibody, Sigma; 1:10,000]; K9JA phosphorylation-independent pan-tau antibody [rabbit polyclonal antibody, Dako; 1:20,000] [56], and detected with anti-mouse or anti-rabbit IgG conjugated to IRDye 680 or 800 (Li-Cor Biosciences; 1:10,000). Western blots were developed using the Odyssey® Imaging System (LI-COR Biosciences), which allows detection of multiple primary antibodies probed on the same blot. Densitometric and MW analyses were performed using ImageJ software (National Institutes of Health). Band density values were normalized to β-actin levels.

Sarkosyl insolubility assay

Extraction of sarkosyl-insoluble tau was performed as previously described [19]. Briefly, whole frozen brains of 24- and 16-month-old rTgTauEC mice were homogenized by polytron in 10 volumes of buffer H (10 mM Tris–HCl [pH 7.5] containing 0.8 M NaCl, 1 mM EGTA, and 1 mM dithiothreitol) and spun at 100,000×*g* for 30 min at 4 °C. Another 2 ml of buffer H was added to the pellet and the samples were homogenized again by polytron, incubated in 1 % Triton X-100 at 37 °C for 30 min. Following the incubation, the samples were spun at 100,000×*g* for 30 min at 4 °C, the pellet was homogenized by polytron in 1 ml of buffer H and was then incubated in 1 % sarkosyl at 37 °C for 30 min, and spun at 100,000×*g* for 30 min at 4 °C. The supernatant was then collected (sarkosyl-soluble fraction). Detergent-insoluble pellets were extracted in 100 μl of urea buffer (8 M urea, 50 mM Tris–HCl [pH 7.5]), sonicated, and spun at 100,000×*g* for 30 min at 4 °C. The supernatant was then collected (sarkosyl-insoluble fraction).

Behavior experiments

Behavioral tests were performed at the NeuroBehavior Laboratory Core at Harvard NeuroDiscovery Center. The experimenter was blind to genotype for all behavioral tests. For detailed methods see Supplemental Methods.

Electrophysiology

Experiments were performed as previously reported with modifications [6, 31, 41]. Animals were deeply anesthetized using isoflurane and killed by decapitation. The brain was quickly removed and dissected in an ice-cold cutting solution. Acute horizontal slices (400 μm) were prepared from non-transgenic controls and rTgTauEC mice at 16 months of age. Slices were cut on a DTK-2000 microslicer (Dosaka) in ice-cold extracellular cutting solution containing the following (in mM): 215 sucrose, 2.5 KCl, 20 glucose, 26 $NaHCO_3$, 1.6 NaH_2PO_4, 1 $CaCl_2$, 4 $MgCl_2$, and 4 $MgSO_4$. Slices were then placed, at room temperature, in a holding chamber containing 50 % cutting solution and 50 % artificial cerebral spinal fluid (CSF) (ACSF) recording solution containing the following (in mm): 124 NaCl, 26 $NaHCO_3$, 10 glucose, 2.5 KCl, 1 NaH_2PO_4, 2.5 $CaCl_2$, and 1.3 $MgSO_4$. After 30 min, the 1:1 solution was switched to ACSF. The slices were kept at room temperature for at least 1 h before being transferred to the recording chamber. Cutting and recording solutions were both saturated with 95 % O_2 and 5 % CO_2, pH 7.4. Experiments were performed at room temperature. A patch-type pipette filled with 1 M NaCl was used to record field excitatory postsynaptic potentials (fEPSPs) and evoked every 20 s with a bipolar tungsten electrode in the presence of 100 μM picrotoxin (Sigma-Aldrich) to block inhibitory transmission.

Data were acquired with Digidata-1322A and digitized at 10 kHz using the pClamp 10 software. Recordings were performed with a MultiClamp 700A amplifier (Axon Instruments), and output signals were filtered at 3 kHz. The data were analyzed using MiniAnalisys (Synaptosoft). The stimulating and recording electrodes were positioned at the same depth in the slice and the distance between them was kept constant (~200 μm). Input/output (I/O) curves were generated using stimulus intensities from 10 to 100 μA in increments of 10 μA and plotted as a function of fiber volley amplitude. Paired-pulse facilitation and depression were assessed using 50 and 100 ms inter-stimulus intervals. Before LTP induction, stable baseline responses were acquired for at least 20 min. LTP was induced at baseline stimulus intensity using high-frequency stimulation (HFS) which consisted of four trains of 50 pulses at 100 Hz with 10 s inter-train intervals. The magnitude of LTP was estimated by comparing averaged responses 15–45 min after induction with baseline-averaged responses before induction. For statistical analysis, responses were collected and every three responses (1 min periods) for the LTP experiments or every five responses for the I/O and PPD/PPF experiments were averaged. fEPSP slope or amplitude were calculated. As previously described, fEPSP were evoked and recorded at CA3-CA1 and PP-DG [18]. For more

detailed electrode placing information see Supplemental material.

Real time quantitative RT-PCR analysis of Arc mRNA

Arc mRNA levels were measured 30 min after rTgTauEC and non-transgenic control mice were re-exposed to CFC (or not exposed) ($n = 5$ or 6 per group). RT-PCR procedure was performed as previously reported with modifications [52]. Animals were killed, their brains removed, and the hippocampus was dissected. Total RNA was extracted from hippocampus by homogenizing tissue in 500 µl of Trizol reagent (Invitrogen) followed by addition of 100 µl chloroform at room temperature and incubated for 10 min. Samples were centrifuged for 15 min at 12,000*g* at 4 °C and the aqueous phase was transferred to new, RNase-free Eppendorf tubes. The RNA was precipitated by addition of 250 µl of isopropanol and frozen for 1 h at −80 °C. These samples were then centrifuged for 15 min at 12,000*g* at 4 °C, the RNA pellets were washed in 70 % EtOH, air-dried for several minutes, and then suspended in 14 µl of UltraPure™ DNase/RNase-Free Distilled Water. RNA samples were assayed for quality with an Agilent 6000 Bioanalyzer and a Nanodrop spectrophotometer. Reverse transcription was carried out on all RNA samples (Superscript II, Invitrogen). The relative amount of *Arc* was normalized to the level of internal control housekeeping gene message for glyceraldehyde-3-phosphate dehydrogenase (GAPDH) mRNA levels. Real-time PCR was performed according to the comparative threshold cycle (CT) method (SmartCycler manufacturer's instructions). Differences in threshold crossing cycle between *Arc* and GAPDH (equal to DeltaCT) were calculated for each condition; then the levels of *Arc* expression were computed as Delta-Delta-CT, *Arc* mRNA levels in CFC exposed, and unexposed transgenic and non-transgenic animals were calculated and normalized to non-transgenic unexposed mice. qPCR analysis (on Bio-Rad iCycler) of the cDNA product was carried out using primers against *Arc* forward, 5′-GAAGGAGTTTCT GCAATACAGTGAG-3′; and reverse, 5′-ACATACTG AATGATCTCCTCCTCCT-3′ and GAPDH forward, 5′-AT GACATCAAGAAGGTGGTG-3′, and reverse, 5′-CATAC CAGGAAATGAGCTTG-3′. Duplicates or triplicates of cDNA samples were added to a 25-µl reaction containing 12.5 µl SYBR green Mastermix (Applied Biotechnology).

Statistical analyses

Normality of data was assessed with a Shapiro–Wilks test. Data were analyzed with appropriate statistics including Student's *t* test, Mann–Whitney test, one-way ANOVA followed by Tukey post hoc test (when necessary), and Kolmogorov–Smirnov test (KS-test). *P* values <0.05 were considered to be statistically significant. Data were reported as mean ± SEM.

Results

To assess tau pathology in rTgTauEC mice we immunostained horizontal brain slices from 9- and 16 month-old animals with different tau antibodies. At 9 months of age, human tau protein (htau) assessed by the human tau-specific antibody Tau13 (that shows no reactivity in control mouse brain, Fig. S1a), has a restricted distribution of htau in the medial entorhinal cortex (MEC) and in the axon terminals in the middle molecular layer (mml) of the dentate gyrus (DG), which receives axons originating in the MEC (Fig. 1a–e; Table 1). At this age only a very small number of Alz50-positive (misfolded tau and a pre-tangle marker) cell bodies (Fig. 1d; Table 1) and Alz50 and PHF1-positive (hyperphosphorylated tau) neurites (Fig. 1d, e) were observed in the EC. The Alz50 staining pattern was confirmed using a different misfolded tau antibody MC1 (Fig. S1b–c). By contrast, 16-month-old rTgTauEC mice show numerous aggregates positive for human tau, Alz50, and PHF1 in the EC cell bodies (Fig. 1f–j). The phenotype of "spreading" of tau to the DG granule cells occurs largely in older mice (21–24 months), although even at 16 months rare granule cells were positive for human tau, Alz50, and PHF1 (Fig. 1o–r). Axons and dendrites, but no soma, were human tau immunopositive in the hippocampus at 9 months of age (Fig. 1k–n). Thus, 16-month-old animals show a different pattern of tau distribution (Fig. 1a, b vs f, g), and the levels of tau are considerably increased (Fig. S1d), consistent with previous reports [9].

The lesions present in the EC at 16 months of age were primarily still pre-tangle in their staining properties. There were only rare Gallyas silver positive neurons in the EC with the density of 9.1 neurons/mm^2 (on the order of 0–5 neurons per slice) (Fig. 2a; Table 1) and no thioflavin S-staining suggesting that the vast majority of the prominent tau positive neurons are in a pre-tangle state. As the animals age, the disease progresses and at 24 months of age the density of Gallyas-positive tangles in the EC increases dramatically to 1,775 ± 534 Gallyas-positive neurons/hemisphere or 26 ± 8.76 number neurons/mm^2. Gallyas-positive neurons in the dentate gyrus at 24 months of age were infrequent, usually <5 per slide. Consistent with pre-tangle pathology, immunoblotting of sarkosyl fractions from 16-month-old rTgTauEC mice revealed very low levels of sarkosyl-insoluble tau species at 55 kDa with most tau detected in the soluble fraction as a 55-kDa species.

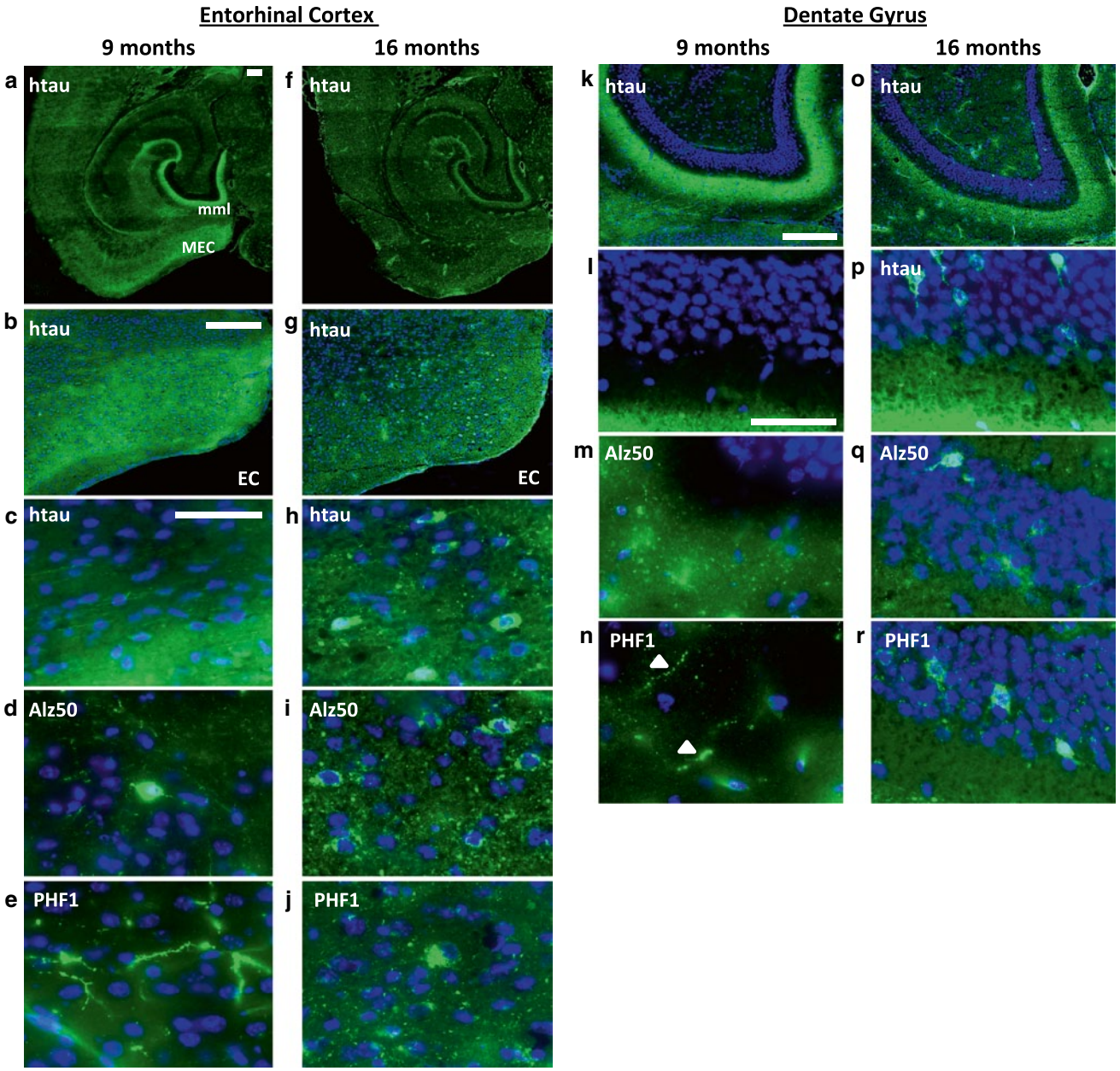

Fig. 1 Distribution of tau in the entorhinal cortex (EC) and dentate gyrus (DG) of rTgTauEC mice at 9 and 16 months of age. EC: **a**, **f** Low magnification view of medial horizontal sections from 9- and 16-month-old rTgTauEC mouse brains showing the distribution of human tau using the human tau specific phosphorylation-independent Tau13 antibody. At 9 months, human tau (htau) has a restricted distribution in the MEC and in the axonal terminals in the middle molecular layer (mml) of the DG **a** (**b**, **c** higher magnifications of the EC). 16-month-old rTgTauEC mice show numerous human tau-positive cell bodies in the EC **f** (**g**, **h** higher magnifications of the EC). Alz50 staining shows rare Alz50-positive EC cell bodies at 9 months (**d**) and a number of Alz50-positive neurons in the EC at 16 months (**i**). Immunohistochemistry using PHF1 shows PHF1-positive neurites in the EC at 9 months (**e**) and PHF1-positive aggregates in the EC neurons of 16-month-old rTgTauEC mice (**j**). DG: At 9 months, human tau (**k**, **l**), Alz50 (**m**) and PHF1 (**n**) staining are limited to mml of the DG. At 16 months, a few granule cells are positive for human tau (**o**, **p**), Alz50 (**q**) and PHF1 (**r**). Tau is shown in green and DAPI nuclei are shown in *blue*. *Scale bars* 200 μm (**a**, **b**, **f**, **g**, **k**, **r**) and 50 μm (**c**–**e**, **h**–**j**). *White arrows* indicate axonal tau staining

A 64-kDa insoluble hyperphosphorylated tau species that could be detected at 24 months [9] was absent in 16-month-old animals' brains (Fig. 2b).

The EC-hippocampus system plays a critical role in memory formation and memory consolidation. We tested the hypothesis that accumulation of tau in the perforant pathway might be associated with cognitive decline. We used the open field test to measure the general locomotor and exploratory activity of rTgTauEC mice. While 9-month-old transgenic mice showed similar total distance

Table 1 Densities of human tau, Alz50 and Gallyas-stained cells in entorhinal cortex and dentate gyrus of 16 month-old rTgTauEC mice ($n = 3$ mice)

	Number (neurons/mm^2)
Entorhinal Cortex	
Human tau	85.22 ± 7.70
Alz50	78.68 ± 8.91
Gallyas	9.1 ± 2.20
Dentate Gyrus	
Human tau	58.96 ± 22.08
Alz50	46.93 ± 2.49

Results are expressed as the mean ± SEM

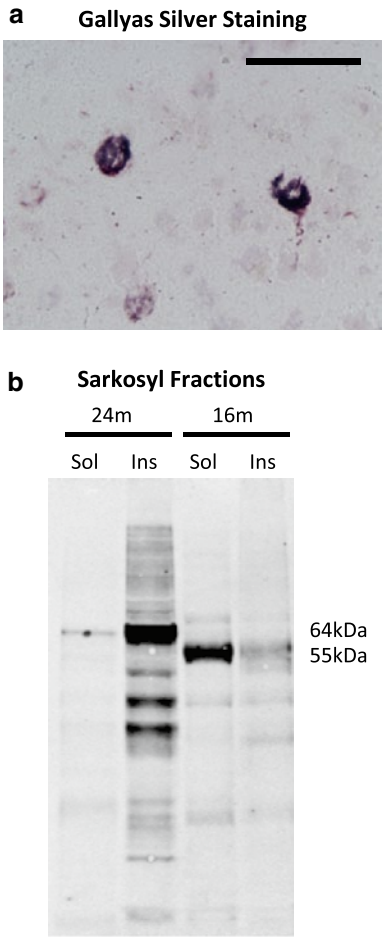

Fig. 2 Rare Gallyas silver-positive tangles in the EC **a** rTgTauEC animals rarely show sporadic silver-positive neurofibrillary tangles in the EC at 16 months of age. *Scale bar* 50 μm. **b** Immunoblotting of sarkosyl fractions from rTgTauEC mice using a K9JA total tau antibody revealed very low levels of sarkosyl insoluble tau species at 55 kDa in 16-month-old mouse with most of tau detected in the soluble fraction as a 55-kDa species of tau. A 64-kDa insoluble hyperphosphorylated tau species detected at 24 months but absent in 16-month-old animals brains

Fig. 3 **a** Open field locomotor and exploratory activity test in rTgTauEC mice revealed no changes in the activity of 9-month-old transgenic mice (control, $n = 12$; rTgTauEC, $n = 12$) and a significant decrease (~20 %) in the total distance travel ($p = 0.014$) of transgenic mice at 16 months of age (control, $n = 6$; rTgTauEC, $n = 14$) compared to age-matched non-transgenic controls. **b** Contextual fear conditioning (CFC) shows no changes in fear response measured by freezing in 9-month-old mice (24 h: control, $n = 6$; rTgTauEC, $n = 14$; 48 h: control, $n = 3$; rTgTauEC, $n = 6$) **c** but 16-month-old rTgTauEC mice (24 h: control, $n = 12$; rTgTauEC, $n = 12$; 48 h: control, $n = 4$; rTgTauEC, $n = 6$) had a small decreased freezing time (48 h) compared to age-matched controls ($p = 0.0414$). **d** Activation of *Arc* mRNA expression induced by hippocampus-dependent fear response to contextual fear conditioning (CFC) was assessed using qRT-PCR. Mice that were re-exposed to CFC 48 h after training and killed 30 min after re-exposure were compared to unexposed mice. **e** 9-month-old controls and transgenic mice re-exposed to CFC show a significant increase in *Arc* mRNA levels in the hippocampus compared to unexposed mice. There was no difference in *Arc* mRNA levels of rTgTauEC mice compared to controls (9 months: control, unexposed $n = 4$, re-exposed $n = 5$; rTgTauEC, unexposed $n = 6$, re-exposed $n = 6$). **f** 16-month-old transgenic mice have significantly less *Arc* activation following CFC re-exposure compared to controls. (16 months: control, unexposed $n = 3$, re-exposed $n = 4$; rTgTauEC, unexposed $n = 3$, re-exposed $n = 6$). Results are expressed as means + SEM. Comparisons between groups were made by *t* test or Mann–Whitney test (for CFC). *Asterisk* indicates statistical significance, $p < 0.05$. For CFC: *Asterisk* indicates statistically significant difference between unexposed and re-exposed mice, $p < 0.05$. *Hash* indicates statistically significant difference between control and transgenic mice, $p < 0.05$. n.s. indicates no statistical significance

traveled compared to age-matched non-transgenic controls (Fig. 3a), at 16 months transgenic mice showed a significant decrease (~20 %) in total distance traveled ($p = 0.014$) (Fig. 3b). There were no changes in the percent distance traveled in the center (Fig. S2a) or in the number of vertical counts (Fig. S2b) suggesting no changes in anxiety levels or exploratory behavior. The 16-month-old animals showed similar latency to fall on the rotarod test compared to controls, consistent with normal motor function (Fig. S2c). Moreover, 16-month-old animals performed similarly to controls on the radial arm maze, a test dependent on the hippocampal formation, showing intact spatial memory (Fig. S2d).

Contextual fear conditioning (CFC) also depends on the limbic system and represents a form of associative learning in which the animal learns to predict aversive events. We assessed the fear response of rTgTauEC mice using a CFC paradigm consisting of 3 days of testing with training (shock delivery) performed on the first day, followed by two additional days of testing (24 and 48 h after training) (Fig. S2e). We found that there were no changes in fear response measured by freezing in 9-month-old rTgTauEC mice compared to controls (Fig. 3c). While 16-month-old rTgTauEC mice had a mild decreased freezing time during

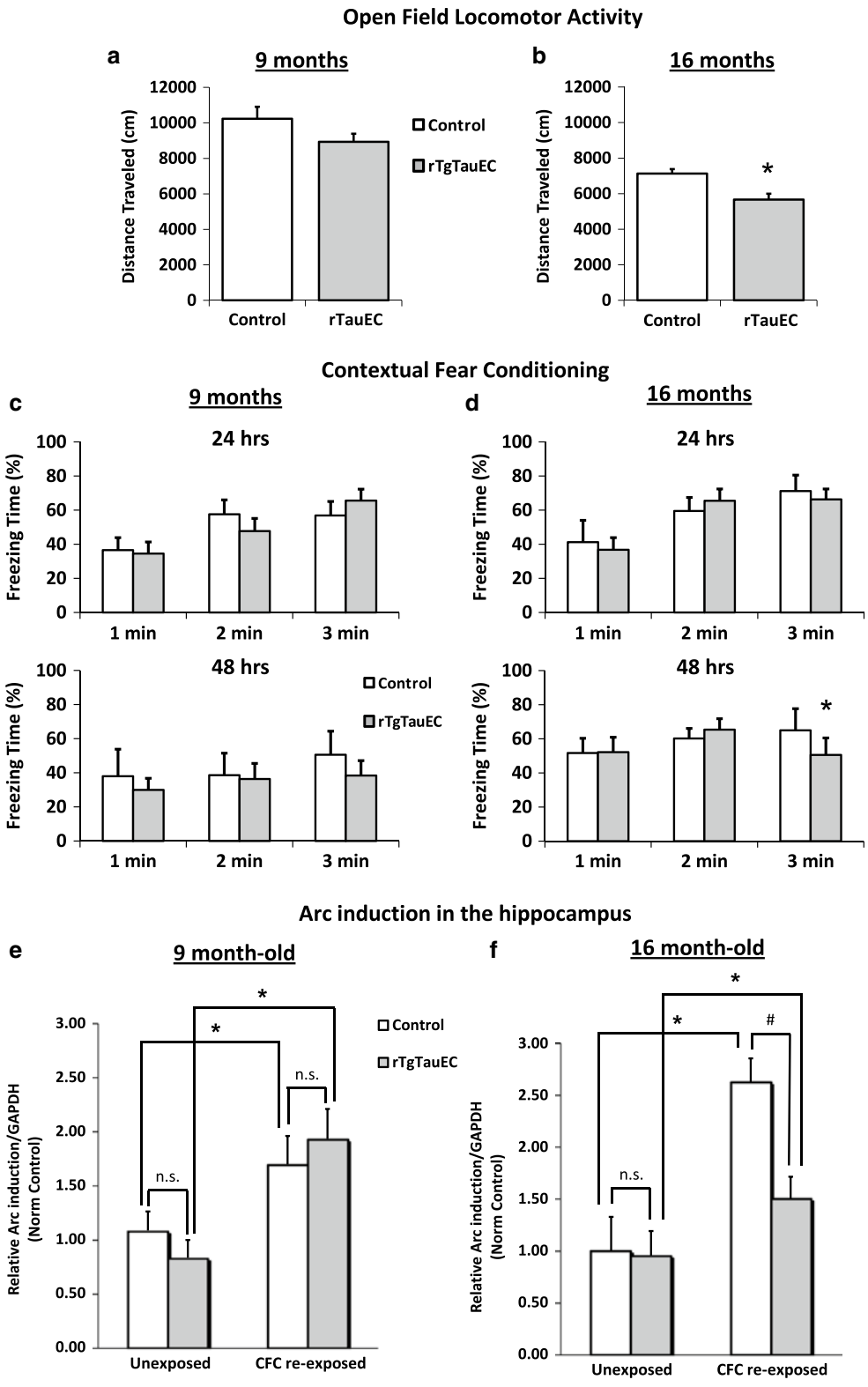

the last minute on the second day of testing (48 h) (Fig. 3d), this represents a mild effect with a small sample size (control, $n = 4$; rTgTauEC, $n = 6$), suggesting nearly normal CFC behavior. There were no differences in the freezing time at baseline (prior to shock delivery) between controls and transgenic mice in either age group (Fig. S2f, g).

Next we assessed whether tau accumulation leads to changes in the activation of the plasticity-related activity

regulated, cytoskeletal-associated gene *Arc,* which is induced in hippocampus-dependent fear conditioning [8, 40]. Both controls and transgenic mice that had been re-exposed to CFC were compared to unexposed mice. We quantified *Arc* mRNA by quantitative real-time polymerase chain reaction (qRT-PCR) in the hippocampus 30 min after CFC behavioral experience. Half the animals that were tested on the CFC task at 24 h after training were re-tested at 48 h and killed 30 min thereafter. mRNA levels were determined in CFC re-exposed and CFC unexposed mice. As expected, in 9-month-old mice there was a significant increase in *Arc* mRNA levels in the hippocampus of both controls ($p = 0.019$) and rTgTauEC transgenic ($p = 0.0087$) mice that had been re-exposed to CFC compared to unexposed mice (Fig. 3e), showing the expected *Arc* induction in response to CFC. No difference in the pattern of *Arc* mRNA levels of rTgTauEC mice compared to controls was observed in animals at 9 months of age, consistent with the observed behavioral results (Fig. 3e). By contrast, 16-month-old transgenic mice showed significantly less *Arc* activation following CFC re-exposure compared to controls (Fig. 3f) ($p = 0.0254$). At 16 months, both controls and rTgTauEC transgenic mice that had been re-exposed to CFC showed a significant increase in *Arc* mRNA levels in the hippocampus compared to unexposed mice ($p = 0.0286$ and $p = 0.0223$, respectively), but the size of the increase of *Arc* transcription was significantly smaller in the transgenic animals by ~57 %.

These results suggest subtle changes in one of the two hippocampal-dependent memory tests assessed in this study as well as changes in the responsiveness of the neural system activity marker *Arc* occur in the rTgTauEC model as they age. To further explore whether human mutant tau overexpression in the EC and perforant pathway impairs synaptic function in the hippocampus, we measured baseline synaptic transmission, short-term plasticity, and long-term potentiation (LTP) at the EC medial perforant pathway to dentate gyrus granule cell synapses (PP-DG) in 16-month-old mice as illustrated by the schematic diagram of the medial perforant pathway with the positioning of the stimulating (S) and recording (R) electrodes (Fig. 4a). Recordings were also performed at the Schaffer collateral synapse to CA1 synapse (CA3–CA1) which we anticipated would be unaffected by EC specific human mutant tau overexpression. We recorded extracellular field excitatory postsynaptic potentials (fEPSP) from horizontal EC-hippocampal slices. To assess baseline synaptic transmission strength we examined the input–output relationship of PP-DG and CA3-CA1 synapses in response to single electrical stimuli and found no significant difference between transgenic and control animals at either synapse when the fEPSP was plotted against the fiber volley amplitude (Fig. 4b; Fig. S3b). There was increased presynaptic volley amplitude in the PP-DG synapse of rTgTauEC mice compared to controls when the fiber volley amplitude was plotted as a function of the stimulus intensity (Fig. 4c), suggesting enhanced axonal excitability and indicative of a presynaptic alteration.

Fig. 4 Synaptic transmission at the EC medial perforant pathway to dentate gyrus granule cell synapses (PP-DG). Extracellular field excitatory postsynaptic potentials (fEPSP) were recorded from horizontal EC-hippocampal slices of 16-month-old rTgTauEC and age-matched non-transgenic controls. **a** Schematic diagram of medial perforant pathway (MPP) synapto-architecture showing middle molecular layer (mml) and granule cells (gl) of the dentate gyrus with the positioning of stimulation (S) and recording (R) electrodes. **b** Typical shape of a fEPSP illustrating the method of assessment of presynaptic fiber volley amplitude and fEPSP slope. **b** Basal synaptic transmission was examined by building input–output (I/O) relationship at the PP-DG synapse in response to single electrical stimuli ranging from 10 to 800 μA and plotted as the relationship between fEPSP slope and fiber volley amplitude, showing no significant difference between transgenic mice compared to control animals. **c** Fiber volley amplitude was plotted as a function of stimulus intensity and it shows a significant increase in fiber volley amplitude for a given stimulus intensity in the rTgTauEC mice compared to controls. (n = [control, $n = 10$ (3); rTgTauEC, $n = 8$ (4)]). **d** Typical shape of a population spike illustrating the method of assessment of amplitude of the population spike and the slope of the EPSP. E–S coupling was assessed by measuring the slope of the initial population EPSP and the amplitude of the population spike. Curves were generated for EPSP slope versus population spike amplitude. There was no change in E–S coupling in rTgTauEC mice compared to controls, the field suggesting that these animals do not have a post-synaptic change. (n = [control, $n = 4$ (3); rTgTauEC, $n = 4$ (3)])

To assess if there are post-synaptic changes in the PP-DG synapse associated with enhanced pre-synaptic axonal excitability, we measured the slope of the initial population EPSP and the amplitude of the population spike as described [59]. This measurement can be used as an indicator of post-synaptic changes since more excitable cells fire action potentials with lower amplitude synaptic input. There was no consistent shift of the EPSP slope versus population spike amplitude curve (E–S coupling) suggesting that these animals do not show a post-synaptic change that can be detected by this measurement (Fig. 4d).

Next we measured paired pulse ratio (PPR) in the PP-DG and CA3-CA1 synapses, a form of short-term plasticity traditionally used as an indirect way to estimate the probability of transmitter release (Pr). PPR is inversely correlated with Pr; synapses with low Pr usually show paired pulse facilitation (PPF), whereas synapses with high Pr show paired-pulse depression (PPD) [36, 53]. We measured PPR in the PP-DG synapse that normally shows PPD, such that a single stimulus leading to synaptic activation will depress a subsequent synaptic response (Fig. 5a). We used two inter-stimulus intervals (ISI) (50 and 100 ms) with equal intensity for both stimuli. We used stimulus intensity

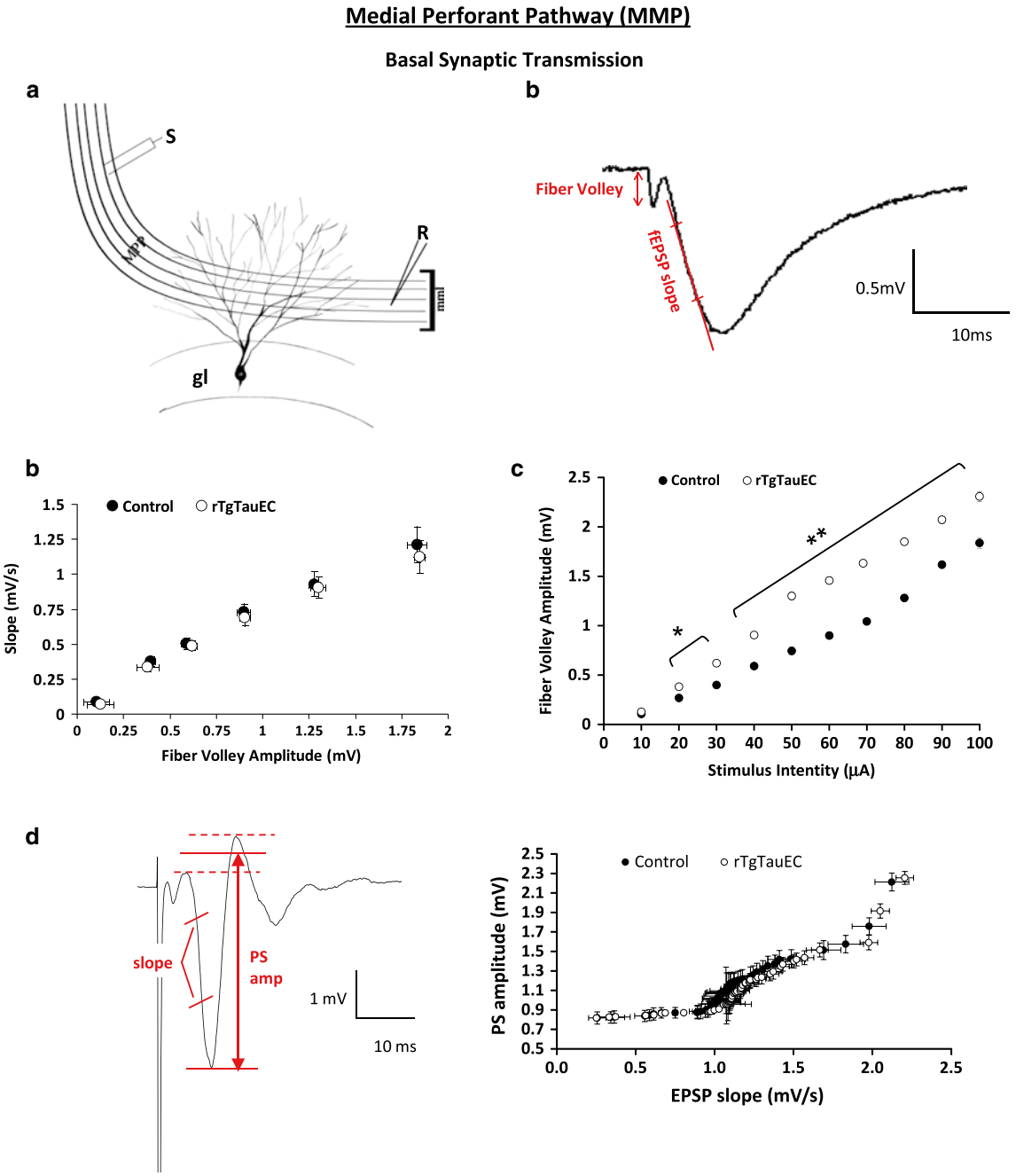

that elicits similar initial fEPSP amplitude in slices from controls and transgenic ranging from 0.9 to 1.5 mV. In slices from transgenic mice, PPD was significantly increased compared to controls, as measured by the PPR (ratio between the amplitude of the second pulse and the first pulse) ($p = 0.0062$ for 50 ms; $p = 0.0007$ for 100 ms). This suggests an increase in the probability of transmitter release in the transgenic mice, consistent with a presynaptic alteration (Fig. 5a).

In contrast to the PP-DG synapse that shows PPD, CA3–CA1 synapses exhibit PPF, such that a single synaptic activation facilitates a subsequent synaptic response. We used 50 and 100 ms ISI and initial amplitude responses ranging from 1.6 to 2 mV. We measured the PPR at the CA3–CA1 synapse and found no changes in PPF in transgenic mice compared to age-matched controls (Fig. S3c) as expected because the transgene is not expressed in this circuit.

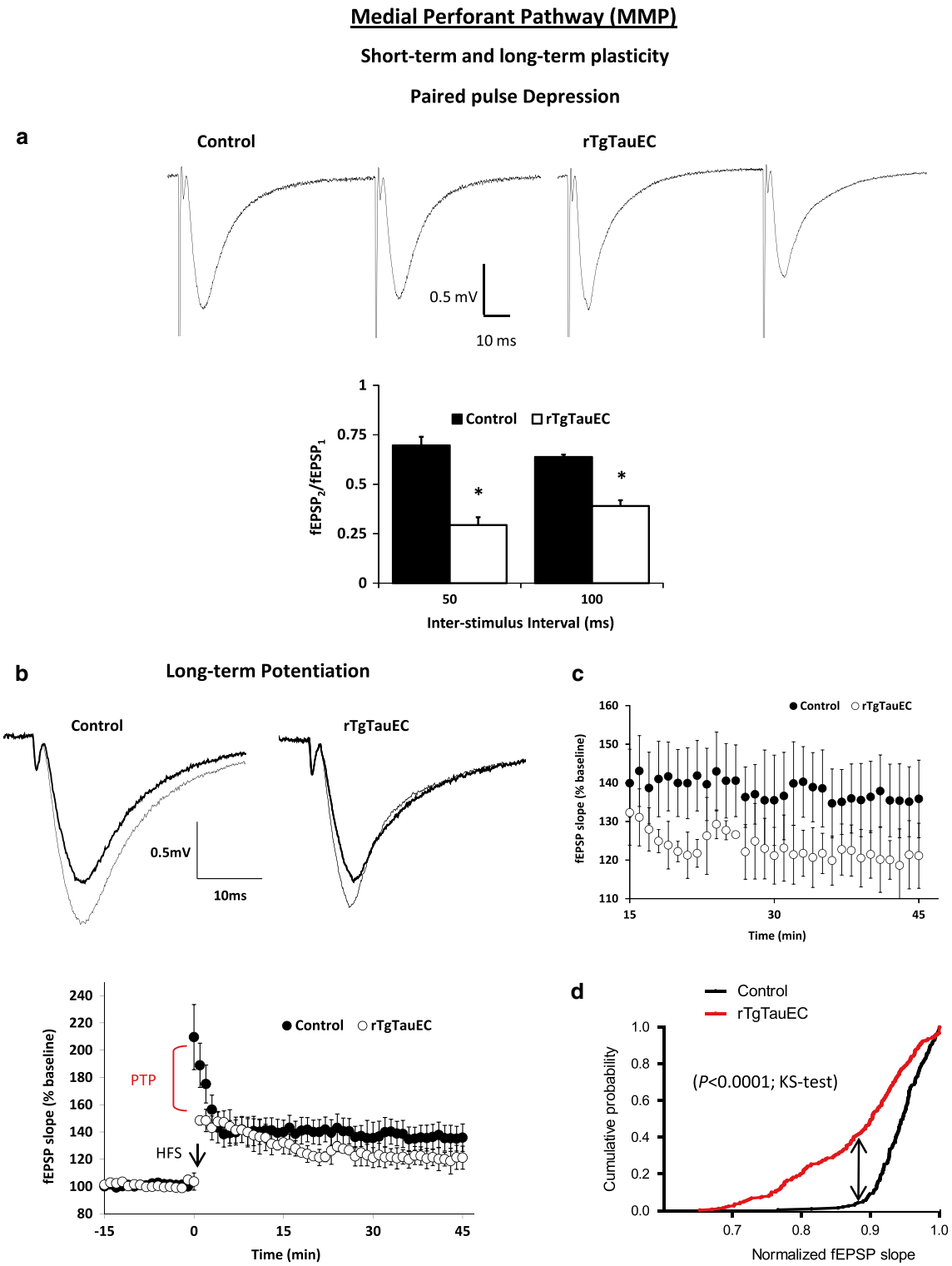

In addition, we assessed whether long-term potentiation (LTP) is altered in the medial perforant pathway rTgTauEC mice (Fig. 5b–d). LTP is a long-lasting strengthening of the response of postsynaptic neurons to high-frequency stimulation and is widely accepted as a critical molecular mechanisms that underlies learning and long-term memory. Post-tetanic potentiation (PTP) is a form of short-term plasticity generally thought to be presynaptic with a mechanism similar to PPF and PPD, in that after high frequency stimulations, often used for LTP induction, there is a high level of residual calcium in the presynaptic cell, temporarily increasing the probability of release. LTP was

◂**Fig. 5** Synaptic plasticity at the medial perforant pathway. **a** Short-term plasticity was evaluated by measuring paired pulse depression (PPD) of the PP-DG synapse. Paired-pulse ratios (PPRs) calculated as the ratio between the amplitude of the second response ($fEPSP_2$) and the first response ($fEPSP_1$) to two pulses delivered either 50 or 100 ms apart. Representative fEPSP for responses with 50 ms interval is shown. There was a significant increase in PPD shown by decreased PPR (n = [control, n = 6 (3); rTgTauEC, n = 6 (4)]). **b–d** LTP was evaluated by comparing fEPSP slopes as a percentage of the pre-tetanus baseline fEPSP slopes (n = [control, n = 6 (3); rTgTauEC, n = 8 (4)]). Representative traces before (*bold line*) and 30–45 min after (*thin line*) the induction. There was a significant reduction in the post-tetanic potentiation (PTP) after high-frequency stimulation (HFS) (**d**). fEPSP responses between 15 and 45 min after HFS are shown in E. Results are expressed as mean ± SEM. *Asterisk* indicates statistical significance, $p < 0.05$ (**b–d**). Comparisons between groups were made by t test (**b–d**). **f** Cumulative probability distribution plots for recordings from 15 to 45 min after LTP induction show a significant decrease in LTP elicited in rTgTauEC mice compared to controls. Comparison between groups was made by Kolmogorov–Smirnov test (KS-test). *Asterisk* indicates statistical significance, $p < 0.05$. (n = [number of slices (number of animals)])

induced after the acquisition of a stable baseline. Baseline fEPSP slope and fiber volley amplitude were kept similar for slices from controls and transgenic mice with fEPSP slope ranging from 0.9 to 1.1 mV/ms and fiber volley 0.75 to 0.95 mV. Slices from transgenic animals demonstrated a significant reduction in PTP after high-frequency stimulation in the PP-DG synapse ($p < 0.0001$) (Fig. 5d). Responses reached a steady state by 15 min after tetanus (Fig. 5e). Cumulative probability plots of response amplitudes 15–45 min following high-frequency stimulation of the medial perforant pathway revealed that LTP was markedly decreased in transgenic mice compared to control mice ($p < 0.0001$) (Fig. 5f). In contrast, tetanic stimulation at the CA3-CA1 synapse elicited unchanged PTP and intact LTP in rTgTauEC slices compared to age-matched controls (Fig. S3d–f).

Discussion

In this study, we addressed the question of whether soluble pathological forms of tau alter neural system integrity independently of overt neurodegeneration or fibrillar NFTs, by studying a middle-aged group of rTauEC mice. This line has the advantage of expressing tau at high levels in a discrete population of neurons in the MEC, and this particular population of neurons gives rise to a focused projection, the perforant pathway, that targets the hippocampus primarily in a very well-defined terminal zone in the middle third of the molecular layer of the dentate gyrus. The perforant pathway accounts for a substantial percentage of cortical- hippocampal input [54]. Thus alterations in neuronal function of this population of neurons might be expected to produce detectable behavioral and physiological alterations, both because the lesions are targeted to an anatomically critical subpopulation of neurons and because highly sensitive techniques have been developed to monitor hippocampal formation function in rodent models. We examined mice at 9 and 16 months of age. The younger mice had detectable expression of the transgene in perforant pathway axons, as expected since tau is normally localized to the axonal compartment, but little accumulation of tau in the soma. The 16-month-old mice had soluble "pathological" forms of tau—marked by immunostaining with the antibodies Alz50, MC1, and PHF1—in the somatodendritic compartment but rare silver positive and no thioflavine S positive NFTs.

We have previously shown that rTgTauEC mice show no evidence of synapse or neuronal loss at 16 months of age and that these phenotypes were only observed at 24 months of age [9]. Alz50, MC1, CP13, AT8, PHF1, and later pathology markers such as Gallyas and ThioS accumulate in the soma as the mice age, beginning approximately at 16 months and progressing to full NFT markers by 24 months [9, 18, 35]. For example, Gallyas silver-positive tau aggregates are not consistently observed in all mice until 18–21 months of age and Thioflavin S (ThioS)-positive mature neurofibrillary tangles are not present until 21–24 months of age. Progression of tau pathology in the rTgTauEC mouse model is similar to that observed in two independently generated equivalent lines [18, 35].

At 16 months, rTgTauEC mice show nearly normal performance on behavioral tasks, suggesting some degree of continued functional competence of the entorhinal-hippocampal circuit. Nonetheless, there was a deficit in recruitment of *Arc*, an immediate early gene implicated in learning and memory, in the hippocampus following CFC, and electrophysiological studies showed defects in presynaptic function. Taken together, these orthogonal lines of evidence support the conclusion that soluble pathological species of tau, independently of fibrillar aggregates, can directly disrupt neural system function.

In the present study, we report a small deficit in locomotor activity in the open field test in older rTgTauEC mice. 16-month-old animals also showed a very subtle difference in one of two hippocampal-dependent tests (contextual fear conditioning). A previous study using an independently generated mouse line equivalent to the rTgTauEC line, with similar extensive tau accumulation in the EC [18], failed to detect behavioral changes at all in animals at 16 months of age. The open field task was not used by Harris and colleagues and in our study we found subtle deficits in fear conditioning only when the animals were tested 48 h after training, a later time point that was not examined in the previous study [18]. Thus behavioral changes in the rTgTauEC mice are difficult to detect, surprising given the observed

changes in the molecular and electrophysiological assays, and perhaps speak of functional redundancy or resiliency of neural circuits to focal, slowly evolving lesions.

The immediate early gene *Arc* is known to be induced by hippocampal-dependent learning and is widely used as a marker of neural system activation [8, 12, 40]. Previous studies of tau overexpressing mice suggested that tau overexpression, by itself, is sufficient to reduce *Arc* induction in behavioral paradigms [14]. We examined *Arc* induction after a strong hippocampal activating behavior—CFC—and measured hippocampal induction of *Arc* using a qPCR approach. Of importance, since the hippocampus itself does not express human tau in this model, any deficits in *Arc* expression in response to hippocampal activation likely reflect the detrimental neural system consequences of human tau expression in the EC. A reduction in *Arc* induction is clearly observed in the hippocampus in 16-month-old transgenic animals. These results provide a molecular marker of hippocampal dysfunction in the 16-month-old transgenic animals.

We then studied electrophysiological properties of the hippocampal formation in the 16-month-old animals. The strongest clue regarding physiological impairment may be the decreased PPD and PTP in the PP-DG, suggestive of an increased probability of neurotransmitter release presynaptically [38]. The mechanism underlying changes in PPD and PTP is uncertain, with four plausible mechanisms: (1) accumulation of Ca^{2+} in the axon terminal [24, 32–34, 43, 53, 60]. Tau aggregates in presynaptic terminals could contribute to altered calcium levels, in agreement with previous in vitro reports suggesting changes in calcium homeostasis due to tau [63]. Interestingly, pathological forms of tau have been implicated in causing changes in calcium homeostatic loss of dendritic spines, altered axonal transport, and impaired trafficking of organelles, particularly mitochondria [1, 13, 14, 16, 28, 40, 41, 55, 56, 59]. Changes in presynaptic function in EC cells burdened with misfolded and PHF tau are consistent with previous observations of presynaptic impairment in mice overexpressing wild-type human tau (htau mice) showing pre-tangle tau pathology with numerous PHF1-positive neurons in the hippocampal [41]. (2) Alternatively, changes in PPD and transmitter release from the presynaptic terminal in rTgTauEC mice can also be attributed to altered size of the readily releasable vesicle pool [10, 13, 37, 46, 48, 49]. In fact, variations in residual presynaptic Ca^{2+} can modify the fraction of vesicles available for immediate release [11, 46, 49, 55]. (3) GABA release and modulation of presynaptic GABAb receptors [22, 27, 58] could also be responsible for variations in PPD and transmitter release in rTgTauEC mice. Finally, changes in PPD could be a consequence of alterations in presynaptic mGluR receptors in rTgTauEC mice [1, 7, 16, 26, 51].

The small changes observed in the basal synaptic transmission with enhanced axonal excitability and normal E–S coupling in rTgTauEC mice are consistent with the anatomical data showing no morphological degeneration of the perforant pathway terminals at 16 months. It should also be noted that previous studies from all three independently generated EC tau expressing lines showed that, as the animals reach older age and begin to undergo degeneration of the perforant pathway axons and develop frank NFT, human tau protein can also be found prominently in the dentate gyrus granule cells, consistent with a trans-synaptic "propagation" at the perforant pathway synapse [9] in animals generally older than 18–21 months. We do not think that this process of tau propagation accounts for the current observations in the 16-month-old mice, since detection of human tau protein in the DG granule cells occurs rarely in 16-month-old mice, and electrophysiological data recorded at the PP-DG synapse implicate presynaptic rather than postsynaptic alterations. Taken together, these data favor the hypothesis that hippocampal system defects are likely due to presynaptic rather than postsynaptic dysfunction. The presence of even rare Alz50 and PHF1 positive DG neurons at 16 months, however, suggests that some tau becomes extra cellular by this age where in principle it may affect synaptic function. Indeed, microdialysis experiments readily detect extracellular tau in the interstitial fluid of transgenic mice overexpressing P301S human tau [61]. Interestingly, it is possible that changes in presynaptic activity in 16-month-old rTgTauEC mice may in fact be responsible for modulating tau release from EC terminals as it has been recently suggested that tau release is stimulated by neuronal activity [42].

In summary, our data suggest that molecular and electrophysiological impairments of the perforant pathway occur in the pre-neurodegeneration, pre-synapse loss, and pre-tangle stage of disease in rTgTauEC. Together these changes argue that the hyperphosphorylated (PHF1 immunoreactive) and misfolded (Alz50 and MC1 immunoreactive) but nonfibrillar tau in the soma, dendrites and axons of the perforant pathway and EC of rTgTauEC mice have clear consequences to neuronal function within the entorhinal-hippocampal network. Understanding the early neuropathological stages of AD is particularly important as new diagnostic approaches will allow targeting AD therapies to a stage of the illness prior to frank neurodegeneration and development of clinical symptoms.

Acknowledgments This work was supported by National Institutes of Health grants: R00AG033670, R21AG03885, R01AG026249-07, 5T32AG00022222, American Health Assistance Foundation, the Glenn Foundation, The Alzheimer's Association Zenith Award ZEN-09-132524, Alzheimer's Research UK, and a portion of the behavioral work was supported by the Harvard NeuroDiscovery Center. We thank Mark Mayford for providing neuropsin-tTA mice, and Peter Davies for providing tau antibodies.

References

1. Bellone C, Luscher C (2005) mGluRs induce a long-term depression in the ventral tegmental area that involves a switch of the subunit composition of AMPA receptors. Eur J Neurosci 21(5):1280–1288. doi:10.1111/j.1460-9568.2005.03979.x
2. Bi M, Ittner A, Ke YD, Gotz J, Ittner LM (2011) Tau-targeted immunization impedes progression of neurofibrillary histopathology in aged P301L tau transgenic mice. PLoS ONE 6(12):e26860. doi:10.1371/journal.pone.0026860
3. Binder LI, Guillozet-Bongaarts AL, Garcia-Sierra F, Berry RW (2005) Tau, tangles, and Alzheimer's disease. Biochim Biophys Acta 1739(2–3):216–223. doi:10.1016/j.bbadis.2004.08.014
4. Braak H, Braak E (1991) Neuropathological stageing of Alzheimer-related changes. Acta Neuropathol 82(4):239–259
5. Carmel G, Mager EM, Binder LI, Kuret J (1996) The structural basis of monoclonal antibody Alz50's selectivity for Alzheimer's disease pathology. J Biol Chem 271(51):32789–32795
6. Chandra S, Fornai F, Kwon HB, Yazdani U, Atasoy D, Liu X, Hammer RE, Battaglia G, German DC, Castillo PE, Sudhof TC (2004) Double-knockout mice for alpha- and beta-synucleins: effect on synaptic functions. Proc Natl Acad Sci USA 101(41):14966–14971. doi:10.1073/pnas.0406283101
7. Chiamulera C, Epping-Jordan MP, Zocchi A, Marcon C, Cottiny C, Tacconi S, Corsi M, Orzi F, Conquet F (2001) Reinforcing and locomotor stimulant effects of cocaine are absent in mGluR5 null mutant mice. Nat Neurosci 4(9):873–874. doi:10.1038/nn0901-873nn0901-873
8. Czerniawski J, Ree F, Chia C, Ramamoorthi K, Kumata Y, Otto TA (2011) The importance of having Arc: expression of the immediate-early gene Arc is required for hippocampus-dependent fear conditioning and blocked by NMDA receptor antagonism. J Neurosci 31(31):11200–11207. doi:10.1523/JNEUROSCI.2211-11.2011
9. de Calignon A, Polydoro M, Suarez-Calvet M, William C, Adamowicz DH, Kopeikina KJ, Pitstick R, Sahara N, Ashe KH, Carlson GA, Spires-Jones TL, Hyman BT (2012) Propagation of tau pathology in a model of early Alzheimer's disease. Neuron 73(4):685–697. doi:10.1016/j.neuron.2011.11.033
10. Debanne D, Guerineau NC, Gahwiler BH, Thompson SM (1996) Paired-pulse facilitation and depression at unitary synapses in rat hippocampus: quantal fluctuation affects subsequent release. J Physiol 491(Pt 1):163–176
11. Dittman JS, Regehr WG (1998) Calcium dependence and recovery kinetics of presynaptic depression at the climbing fiber to Purkinje cell synapse. J Neurosci 18(16):6147–6162
12. Ebert DH, Greenberg ME (2013) Activity-dependent neuronal signalling and autism spectrum disorder. Nature 493(7432):327–337. doi:10.1038/nature11860
13. Elmqvist D, Quastel DM (1965) A quantitative study of end-plate potentials in isolated human muscle. J Physiol 178(3):505–529
14. Fox LM, William CM, Adamowicz DH, Pitstick R, Carlson GA, Spires-Jones TL, Hyman BT (2011) Soluble tau species, not neurofibrillary aggregates, disrupt neural system integration in a tau transgenic model. J Neuropathol Exp Neurol 70(7):588–595. doi:10.1097/NEN.0b013e318220a658
15. Gallyas F (1971) Silver staining of Alzheimer's neurofibrillary changes by means of physical development. Acta Morphol Acad Sci Hung 19(1):1–8
16. Ghasemzadeh MB, Permenter LK, Lake R, Worley PF, Kalivas PW (2003) Homer1 proteins and AMPA receptors modulate cocaine-induced behavioural plasticity. Eur J Neurosci 18(6):1645–1651. doi:2880
17. Greenberg SG, Davies P, Schein JD, Binder LI (1992) Hydrofluoric acid-treated tau PHF proteins display the same biochemical properties as normal tau. J Biol Chem 267(1):564–569
18. Harris JA, Koyama A, Maeda S, Ho K, Devidze N, Dubal DB, Yu GQ, Masliah E, Mucke L (2012) Human P301L-mutant tau expression in mouse entorhinal-hippocampal network causes tau aggregation and presynaptic pathology but no cognitive deficits. PLoS ONE 7(9):e45881. doi:10.1371/journal.pone.0045881
19. Hasegawa M, Arai T, Akiyama H, Nonaka T, Mori H, Hashimoto T, Yamazaki M, Oyanagi K (2007) TDP-43 is deposited in the Guam parkinsonism-dementia complex brains. Brain 130(Pt 5):1386–1394. doi:10.1093/brain/awm065
20. Hyman BT, Van Hoesen GW, Damasio AR, Barnes CL (1984) Alzheimer's disease: cell-specific pathology isolates the hippocampal formation. Science 225(4667):1168–1170
21. Ingelsson M, Fukumoto H, Newell KL, Growdon JH, Hedley-Whyte ET, Frosch MP, Albert MS, Hyman BT, Irizarry MC (2004) Early Abeta accumulation and progressive synaptic loss, gliosis, and tangle formation in AD brain. Neurology 62(6):925–931
22. Jiang L, Sun S, Nedergaard M, Kang J (2000) Paired-pulse modulation at individual GABAergic synapses in rat hippocampus. J Physiol 523(Pt 2):425–439 PHY_0118 [pii]
23. Jicha GA, Bowser R, Kazam IG, Davies P (1997) Alz-50 and MC-1, a new monoclonal antibody raised to paired helical filaments, recognize conformational epitopes on recombinant tau. J Neurosci Res 48(2):128–132. doi:10.1002/(SICI)1097-4547(19970415)48:2<128:AID-JNR5>3.0.CO;2-E
24. Katz B, Miledi R (1968) The role of calcium in neuromuscular facilitation. J Physiol 195(2):481–492
25. Ke YD, Dramiga J, Schutz U, Kril JJ, Ittner LM, Schroder H, Gotz J (2012) Tau-mediated nuclear depletion and cytoplasmic accumulation of SFPQ in Alzheimer's and Pick's disease. PLoS ONE 7(4):e35678. doi:10.1371/journal.pone.0035678
26. Kim JH, Vezina P (1998) Metabotropic glutamate receptors are necessary for sensitization by amphetamine. Neuro Report 9(3):403–406
27. Kirischuk S, Clements JD, Grantyn R (2002) Presynaptic and postsynaptic mechanisms underlie paired pulse depression at single GABAergic boutons in rat collicular cultures. J Physiol 543(Pt 1):99–116 PHY_021576 [pii]
28. Kopeikina KJ, Carlson GA, Pitstick R, Ludvigson AE, Peters A, Luebke JI, Koffie RM, Frosch MP, Hyman BT, Spires-Jones TL (2011) Tau accumulation causes mitochondrial distribution deficits in neurons in a mouse model of tauopathy and in human Alzheimer's disease brain. Am J Pathol 179(4):2071–2082. doi:10.1016/j.ajpath.2011.07.004
29. Kopeikina KJ, Hyman BT, Spires-Jones TL (2012) Soluble forms of tau are toxic in Alzheimer's disease. Trans Neurosci 3(3):223–233. doi:10.2478/s13380-012-0032-y
30. Ksiezak-Reding H, Davies P, Yen SH (1988) Alz 50, a monoclonal antibody to Alzheimer's disease antigen, cross-reacts with tau proteins from bovine and normal human brain. J Biol Chem 263(17):7943–7947
31. Kwon HB, Castillo PE (2008) Long-term potentiation selectively expressed by NMDA receptors at hippocampal mossy fiber synapses. Neuron 57(1):108–120. doi:10.1016/j.neuron.2007.11.024
32. Lee D, Lee KH, Ho WK, Lee SH (2007) Target cell-specific involvement of presynaptic mitochondria in post-tetanic potentiation at hippocampal mossy fiber synapses. J Neurosci 27(50):13603–13613. doi:10.1523/JNEUROSCI.3985-07.2007
33. Lee JS, Kim MH, Ho WK, Lee SH (2008) Presynaptic release probability and readily releasable pool size are regulated by two independent mechanisms during posttetanic potentiation at the calyx of Held synapse. J Neurosci 28(32):7945–7953. doi:10.1523/JNEUROSCI.2165-08.2008
34. Lee SH, Kim MH, Lee JY, Lee D, Park KH, Ho WK (2007) Na +/Ca2 + exchange and Ca2 + homeostasis in axon terminals

of mammalian central neurons. Ann N Y Acad Sci 1099:396–412. doi:1099/1/39610.1196/annals.1387.011
35. Liu L, Drouet V, Wu JW, Witter MP, Small SA, Clelland C, Duff K (2012) Trans-synaptic spread of tau pathology in vivo. PLoS ONE 7(2):e31302. doi:10.1371/journal.pone.0031302
36. Manabe T, Wyllie DJ, Perkel DJ, Nicoll RA (1993) Modulation of synaptic transmission and long-term potentiation: effects on paired pulse facilitation and EPSC variance in the CA1 region of the hippocampus. J Neurophysiol 70(4):1451–1459
37. Mennerick S, Zorumski CF (1995) Presynaptic influence on the time course of fast excitatory synaptic currents in cultured hippocampal cells. J Neurosci 15(4):3178–3192
38. O'Donovan MJ, Rinzel J (1997) Synaptic depression: a dynamic regulator of synaptic communication with varied functional roles. Trends Neurosci 20(10):431–433 S0166-2236(97)01124-7 [pii]
39. Otvos L Jr, Feiner L, Lang E, Szendrei GI, Goedert M, Lee VM (1994) Monoclonal antibody PHF-1 recognizes tau protein phosphorylated at serine residues 396 and 404. J Neurosci Res 39(6):669–673. doi:10.1002/jnr.490390607
40. Plath N, Ohana O, Dammermann B, Errington ML, Schmitz D, Gross C, Mao X, Engelsberg A, Mahlke C, Welzl H, Kobalz U, Stawrakakis A, Fernandez E, Waltereit R, Bick-Sander A, Therstappen E, Cooke SF, Blanquet V, Wurst W, Salmen B, Bosl MR, Lipp HP, Grant SG, Bliss TV, Wolfer DP, Kuhl D (2006) Arc/Arg3.1 is essential for the consolidation of synaptic plasticity and memories. Neuron 52(3):437–444. doi:10.1016/j.neuron.2006.08.024
41. Polydoro M, Acker CM, Duff K, Castillo PE, Davies P (2009) Age-dependent impairment of cognitive and synaptic function in the htau mouse model of tau pathology. J Neurosci 29(34):10741–10749. doi:10.1523/JNEUROSCI.1065-09.2009
42. Pooler AM, Phillips EC, Lau DH, Noble W, Hanger DP (2013) Physiological release of endogenous tau is stimulated by neuronal activity. EMBO Rep 14(4):389–394. doi:10.1038/embor.2013.15
43. Prescott SA (1998) Interactions between depression and facilitation within neural networks: updating the dual-process theory of plasticity. Learn Mem 5(6):446–466
44. Quintanilla RA, Matthews-Roberson TA, Dolan PJ, Johnson GV (2009) Caspase-cleaved tau expression induces mitochondrial dysfunction in immortalized cortical neurons: implications for the pathogenesis of Alzheimer disease. J Biol Chem 284(28):18754–18766. doi:10.1074/jbc.M808908200
45. Rocher AB, Crimins JL, Amatrudo JM, Kinson MS, Todd-Brown MA, Lewis J, Luebke JI (2010) Structural and functional changes in tau mutant mice neurons are not linked to the presence of NFTs. Exp Neurol 223(2):385–393. doi:10.1016/j.expneurol.2009.07.029
46. Sakaba T, Neher E (2001) Quantitative relationship between transmitter release and calcium current at the calyx of held synapse. J Neurosci 21(2):462–476. doi:21/2/462
47. Santacruz K, Lewis J, Spires T, Paulson J, Kotilinek L, Ingelsson M, Guimaraes A, DeTure M, Ramsden M, McGowan E, Forster C, Yue M, Orne J, Janus C, Mariash A, Kuskowski M, Hyman B, Hutton M, Ashe KH (2005) Tau suppression in a neurodegenerative mouse model improves memory function. Science 309(5733):476–481. doi:10.1126/science.1113694
48. Stevens CF, Tsujimoto T (1995) Estimates for the pool size of releasable quanta at a single central synapse and for the time required to refill the pool. Proc Natl Acad Sci USA 92(3):846–849
49. Stevens CF, Wesseling JF (1998) Activity-dependent modulation of the rate at which synaptic vesicles become available to undergo exocytosis. Neuron 21(2):415–424 S0896-6273(00)80550-4 [pii]
50. Swerdlow RH, Burns JM, Khan SM (2010) The Alzheimer's disease mitochondrial cascade hypothesis. J Alzheimers Dis 20(Suppl 2):S265–S279. doi:10.3233/JAD-2010-100339
51. Szumlinski KK, Toda S, Middaugh LD, Worley PF, Kalivas PW (2003) Evidence for a relationship between Group 1 mGluR hypofunction and increased cocaine and ethanol sensitivity in Homer2 null mutant mice. Ann N Y Acad Sci 1003:468–471
52. Tagawa Y, Kanold PO, Majdan M, Shatz CJ (2005) Multiple periods of functional ocular dominance plasticity in mouse visual cortex. Nat Neurosci 8(3):380–388. doi:10.1038/nn1410
53. Thomson AM (2000) Facilitation, augmentation and potentiation at central synapses. Trends Neurosci 23(7):305–312 S0166-2236(00)01580-0 [pii]
54. Van Hoesen GW, Pandya DN, Butters N (1972) Cortical afferents to the entorhinal cortex of the Rhesus monkey. Science 175(4029):1471–1473
55. Wang LY, Kaczmarek LK (1998) High-frequency firing helps replenish the readily releasable pool of synaptic vesicles. Nature 394(6691):384–388. doi:10.1038/28645
56. Wang YP, Biernat J, Pickhardt M, Mandelkow E, Mandelkow EM (2007) Stepwise proteolysis liberates tau fragments that nucleate the Alzheimer-like aggregation of full-length tau in a neuronal cell model. Proc Natl Acad Sci USA 104(24):10252–10257. doi:10.1073/pnas.0703676104
57. Weaver CL, Espinoza M, Kress Y, Davies P (2000) Conformational change as one of the earliest alterations of tau in Alzheimer's disease. Neurobiol Aging 21(5):719–727 S0197-4580(00)00157-3 [pii]
58. Wilcox KS, Dichter MA (1994) Paired pulse depression in cultured hippocampal neurons is due to a presynaptic mechanism independent of GABAB autoreceptor activation. J Neurosci 14(3 Pt 2):1775–1788
59. Xiong ZQ, Stringer JL (1997) Effects of felbamate, gabapentin and lamotrigine on seizure parameters and excitability in the rat hippocampus. Epilepsy Res 27(3):187–194 S0920-1211(97)00022-3 [pii]
60. Xu J, He L, Wu LG (2007) Role of Ca(2+) channels in short-term synaptic plasticity. Curr Opin Neurobiol 17(3):352–359. doi:10.1016/j.conb.2007.04.005
61. Yamada K, Cirrito JR, Stewart FR, Jiang H, Finn MB, Holmes BB, Binder LI, Mandelkow EM, Diamond MI, Lee VM, Holtzman DM (2011) In vivo microdialysis reveals age-dependent decrease of brain interstitial fluid tau levels in P301S human tau transgenic mice. J Neurosci 31(37):13110–13117. doi:10.1523/JNEUROSCI.2569-11.2011
62. Yasuda M, Mayford MR (2006) CaMKII activation in the entorhinal cortex disrupts previously encoded spatial memory. Neuron 50(2):309–318. doi:10.1016/j.neuron.2006.03.035
63. Zempel H, Thies E, Mandelkow E, Mandelkow EM (2010) Abeta oligomers cause localized Ca(2+) elevation, missorting of endogenous Tau into dendrites, Tau phosphorylation, and destruction of microtubules and spines. J Neurosci 30(36):11938–11950. doi:10.1523/JNEUROSCI.2357-10.2010